Ship Detection in SAR Imagery via Variational Bayesian Inference

Shengli Song, Bin Xu, Zenghui Li, and Jian Yang, *Senior Member, IEEE*

***Abstract*—In this letter, we propose a novel ship detection method in synthetic aperture radar (SAR) imagery via variational Bayesian inference. First, we establish the ship detection probabilistic model which decomposes the SAR image as the sum of a sparse component associated with ships and a sea clutter component. Then, we introduce hierarchical priors of the latent variables in the model and use variational Bayesian inference to estimate the posterior distributions of the latent variables. The proposed method is an automatic iterative process without any sliding window. Experimental results accomplished over synthetic data and a RADARSAT-2 SAR image demonstrate that the proposed method can achieve state-of-the-art ship detection performance.**

***Index Terms*—Ship detection, synthetic aperture radar (SAR), variational Bayesian inference.**

I. Introduction

SHIP detection is an important operational topic in the context of synthetic aperture radar (SAR) applications. The constant false-alarm rate (CFAR) detector [1] is a widely used ship detection approach. In this method, sliding windows (including target area, guard area, and background area) are typically used, and the clutter distribution is locally estimated using the samples in the background area. Then, an adaptive threshold is obtained according to a given probability of false alarm (Pfa).

In practical application, the size of sliding windows is generally set according to the size of the ships and the properties of the SAR image (e.g., pixel size and resolution). However, in a multitarget situation, unsuitable sliding-window setups will degrade the performance of ship detection. If there exist multiple targets, the background area of a sliding window may include the pixels of other targets. In this case, the mean and variance of the clutter distribution will be overestimated, leading to the missed detection of weak targets. To solve this problem, Bisceglie and Galdi [2] proposed the order-statistics CFAR detector, which censors out the target pixels from the samples in the background area before the estimation of the clutter distribution. Gao *et al.* [3] proposed a censoring approach based on an empirical parameter called censoring depth; however, the optimal value is hard to obtain. Recently, An *et al.* [4] proposed a global sorting detector based on the iterative censoring scheme [5]. However, this method is mainly used for homogeneous areas. In addition, a method based on subaperture cross-correlation magnitude is proposed in [6]. Then, subband extraction strategy is further studied in [7]. However, subaperture processing in such methods will degrade the spatial resolution and is unfavorable to detect small ships.

In this letter, we propose a novel method based on variational Bayesian inference. Unlike the methods mentioned earlier, the proposed method is not a CFAR detector and does not need sliding windows. Based on the assumption that sparsely distributed ships on sea surface have an intrinsic sparse property, we can decompose the SAR image as the sum of a sparse ship component and a sea clutter component. Then, we establish the ship detection probabilistic model, introducing hierarchical priors on the latent variables and using variational Bayesian inference to estimate the corresponding posterior distributions. The retrieval of the latent variables at each pixel uses all the pixel values in the image; thus, no sliding window is needed.

The letter is organized as follows. Section II introduces the ship detection probabilistic model. The variational Bayesian inference process is described in Section III. Section IV presents the experimental results. Finally, conclusions are drawn in Section V.

II. Ship Detection Probabilistic Model

In SAR images, ships appear as sparsely distributed target pixels with a remarkable sparse characteristic. In addition, sea clutter pixel values are randomly variant. Thus, we can consider ship detection as a sparse signal recovery problem from sea clutter, where an $m \times n$ SAR image can be modeled as

$$\mathbf{D} = \mathbf{A} \circ \mathbf{S} + \mathbf{C}. \tag{1}$$

$\mathbf{D}$, $\mathbf{A} \circ \mathbf{S}$, and $\mathbf{C}$ denote the SAR image, strictly sparse ship component, and sea clutter component, respectively. $\mathbf{A} = [a_{ij}]$ is a binary matrix, with the (i, j)th element $a_{ij} = 1$ indicating the ship pixel, so $\mathbf{A}$ is taken as the ship detection result. $\mathbf{S} = [s_{ij}]$ is the nonstrictly sparse ship component matrix, and $\circ$ denotes the Hadamard (pointwise) product. It should be noted that $c_{ij} = 0$ if $a_{ij} = 1$ in this model.

$\mathbf{A}$, $\mathbf{S}$, and $\mathbf{C}$ are estimated under the Bayesian inference framework. In order to improve the modeling ability to detect the sparse ship component in complicated scenarios, independent priors of a_{ij}, s_{ij}, can consider ship detection and c_{ij} are introduced as follows.

Manuscript received September 3, 2015; revised October 29, 2015, December 2, 2015, and December 16, 2015; accepted December 16, 2015. Date of publication January 12, 2016; date of current version February 24, 2016. This work was supported in part by the National Natural Science Foundation of China (NSFC) under Grant 41171317, by the Key Project of the NSFC under Grant 61132008, by the Major Research Plan of the NSFC under Grant 61490693, and by the Aviation Research Foundation.

S. Song is with the Department of Electronic Engineering, Tsinghua University, Beijing 100084, China, and also with the Luoyang Electronic Equipment Test Center, Luoyang 471000, China (e-mail: ssl_1980@126.com).

B. Xu, Z. Li, and J. Yang are with the Department of Electronic Engineering, Tsinghua University, Beijing 100084, China (e-mail: xubin07161@gmail.com; sunshinenudt@gmail.com; yangjian_ee@mail.tsinghua.edu.cn).

Color versions of one or more of the figures in this paper are available online at http://ieeexplore.ieee.org.

Digital Object Identifier 10.1109/LGRS.2015.2510378

1545-598X © 2016 IEEE. Personal use is permitted, but republication/redistribution requires IEEE permission.
See http://www.ieee.org/publications_standards/publications/rights/index.html for more information.

A. Sparse Component $\mathbf{A} \circ \mathbf{S}$

The binary label coefficient a_{ij} is modeled as [9]

$$\begin{aligned} \mathrm{p}(a_{ij}|e_{ij}) &= e_{ij}^{a_{ij}}(1-e_{ij})^{1-a_{ij}} \\ \mathrm{p}(e_{ij}) &= \mathrm{Beta}(\alpha_0, \beta_0) \end{aligned} \tag{2}$$

where e_{ij} denotes the existence probability of a ship pixel, $\alpha_0 > 0$ and $\beta_0 > 0$ are hyperparameters, and $\mathrm{Beta}(\cdot)$ denotes the Beta distribution. Thus, we have $\mathbb{E}(e_{ij}) = \alpha_0/(\alpha_0+\beta_0)$, where $\mathbb{E}(\cdot)$ denotes the expectation of a random variable. Supposing that $\alpha_0 \ll 1$, $\alpha_0 + \beta_0 = 1$, and then, we can obtain that e_{ij} is close to zero. In this case, sparseness is explicitly imposed on $\mathbf{A}$. It should be noted that α_0 and β_0 do not depend on other parameters. They are set to be deterministic values, and so do the other hypermeters in the following.

The ship pixel s_{ij} is modeled by Gaussian distribution [10]

$$\mathrm{p}(s_{ij}|\mu_{ij}, \lambda_{ij}) = \mathcal{N}\left(s_{ij}|\mu_{ij}, \lambda_{ij}^{-1}\right) \tag{3}$$

where μ_{ij} and λ_{ij} denote the mean and precision of the Gaussian distribution $\mathcal{N}(\cdot)$, respectively.

We further introduce an independent Gaussian-Gamma prior to govern μ_{ij} and λ_{ij} [12]

$$\mathrm{p}(\mu_{ij}, \lambda_{ij}) = \mathcal{N}\left(\mu_{ij}|\mu_{0ij}, \beta_1^{-1}\lambda_{ij}^{-1}\right) \cdot \mathrm{Gam}(\lambda_{ij}|\alpha_1, \gamma_1) \tag{4}$$

where μ_{0ij} is the mean of the Gaussian distribution, $\mathrm{Gam}(\cdot)$ denotes the Gamma distribution, and the hyperparameters α_1, β_1, and γ_1 are set to be small deterministic values to obtain broad hyperpriors.

B. Sea Clutter Component $\mathbf{C}$

In a CFAR detector, the sea clutter is usually modeled by a certain unimodal probabilistic distribution, such as a Gamma distribution, K distribution, and so on. However, in some scenarios, e.g., strongly windy sea areas or heavy rainy sea areas mentioned in [4], the statistic features of the sea clutter over the whole image are spatially variant [4]; thus, the sea clutter distribution may have multimodality. In general, a continuous probability density distribution can be approximated by the mixture of Gaussian (MOG) distribution [12]. Therefore, to better fit the sea clutter distribution in complex sea states, the distribution of c_{ij} is modeled by K-component MOG [8], [12]

$$\begin{aligned} \mathrm{p}(c_{ij}|\boldsymbol{\omega}, \boldsymbol{\tau}, \mathbf{z}_{ij}) &= \prod_{k=1}^{K} \mathcal{N}\left(c_{ij}|\omega_k, \tau_k^{-1}\right)^{z_{ijk}} \\ \mathrm{p}(\mathbf{z}_{ij}|\boldsymbol{\pi}) &= \prod_{k=1}^{K} \pi_k^{z_{ijk}} \end{aligned} \tag{5}$$

where $\mathbf{z}_{ij}$ is a 1-of-K indicator vector associated with c_{ij}, i.e., $z_{ijk} \in \{0,1\}$, $\sum_{k=1}^{K} z_{ijk} = 1$. $\boldsymbol{\pi} = (\pi_1, \ldots, \pi_K)$ is the mixing coefficient vector, with π_k denoting the existence probability of the kth Gaussian component, where $\boldsymbol{\pi}$ satisfies $0 \le \pi_k \le 1$ and $\sum_{k=1}^{K} \pi_k = 1$. $\boldsymbol{\omega} = (\omega_1, \ldots, \omega_K)$ and $\boldsymbol{\tau} = (\tau_1, \ldots, \tau_K)$, where ω_k and τ_k are the mean and precision of the kth Gaussian component, respectively. Here, we simply let $\mathbf{Z}$ denote a $m \times n \times K$ array with the (i,j,k)th element denoted by z_{ijk} to facilitate the following description.

The parameters ω_k and τ_k are also modeled by the Gaussian-Gamma distribution [12]

$$\mathrm{p}(\omega_k, \tau_k) = \mathcal{N}\left(\omega_k|\omega_{0k}, \beta_2^{-1}\tau_k^{-1}\right) \cdot \mathrm{Gam}(\tau_k|\alpha_2, \gamma_2) \tag{6}$$

where ω_{0k} is the mean of the kth Gaussian component; the hyperparameters α_2, β_2, and γ_2 are also set to be small deterministic values.

The Dirichlet distribution is chosen to model the mixing coefficient $\boldsymbol{\pi}$ [12]

$$\mathrm{p}(\boldsymbol{\pi}) = \frac{\Gamma\left(\widehat{\eta_0}\right)}{\Gamma(\eta_{01}) \cdots \Gamma(\eta_{0K})} \prod_{k=1}^{K} \pi_k^{\eta_{0k}-1}, \widehat{\eta_0} = \sum_{k=1}^{K} \eta_{0k} \tag{7}$$

where $\Gamma(\cdot)$ is the gamma function; $\{\eta_{0k}\}$ are hyperparameters, and they are set to small deterministic values.

Based on the probabilistic distributions assumed earlier, the joint distribution of the latent variables $\mathbf{A}$, $\mathbf{E} = [e_{ij}]$, $\mathbf{S}$, $\mathbf{M} = [\mu_{ij}]$, $\boldsymbol{\Lambda} = [\lambda_{ij}]$, $\boldsymbol{\omega}$, $\boldsymbol{\tau}$, $\mathbf{Z}$, $\boldsymbol{\pi}$ and SAR image data $\mathbf{D} = [d_{ij}]$ is expressed as

$$\begin{aligned} &\mathrm{p}(\mathbf{D}, \mathbf{A}, \mathbf{E}, \mathbf{S}, \mathbf{M}, \boldsymbol{\Lambda}, \boldsymbol{\omega}, \boldsymbol{\tau}, \mathbf{Z}, \boldsymbol{\pi}) \\ &\quad = \mathrm{p}(\mathbf{D}|\mathbf{A}, \mathbf{E}, \mathbf{S}, \mathbf{M}, \boldsymbol{\Lambda}, \boldsymbol{\omega}, \boldsymbol{\tau}, \mathbf{Z}, \boldsymbol{\pi})\mathrm{p}(\mathbf{A}|\mathbf{E})\mathrm{p}(\mathbf{E}) \\ &\qquad \cdot \mathrm{p}(\mathbf{S}|\mathbf{M}, \boldsymbol{\Lambda})\mathrm{p}(\mathbf{M}, \boldsymbol{\Lambda})\mathrm{p}(\boldsymbol{\omega}, \boldsymbol{\tau})\mathrm{p}(\mathbf{Z}|\boldsymbol{\pi})\mathrm{p}\boldsymbol{\pi}) \\ &\quad = \prod_{i,j,k} \mathrm{p}(d_{ij}|a_{ij}, e_{ij}, s_{ij}, \mu_{ij}, \lambda_{ij}, \omega_k, \tau_k, z_{ijk}, \pi_k) \\ &\qquad \cdot \mathrm{p}(a_{ij}|e_{ij})\mathrm{p}(e_{ij})\mathrm{p}(s_{ij}|\mu_{ij}, \lambda_{ij})\mathrm{p}(\mu_{ij}, \lambda_{ij}) \\ &\qquad \cdot \mathrm{p}(\omega_k, \tau_k)\mathrm{p}(z_{ijk}|\pi_k)\mathrm{p}(\pi_k). \end{aligned} \tag{8}$$

III. Method Using Variational Bayesian Inference

Variational Bayesian inference is an approximation method with low computational complexity in Bayesian inference theory. Although such method may sometimes find a local optimal solution, a proper initialization can always ensure the desired result.

Variational Bayesian inference is used to compute the posterior distribution approximation $\mathrm{q}(\mathbf{Y})$ for the true posterior $\mathrm{p}(\mathbf{Y}|\mathbf{X})$ by minimizing the Kullback–Leibler (KL) divergence [12], where $\mathbf{Y}$ and $\mathbf{X}$ denote the latent and observed data variables, respectively. In fact, minimizing different divergence functions will result in different approximations. Supposing that we minimize the reverse KL divergence, $\mathrm{q}(\mathbf{Y})$ will place significant probability mass in regions of variable space that have very low probability. However, $\mathrm{q}(\mathbf{Y})$ obtained by minimizing the KL divergence can avoid regions where $\mathrm{p}(\mathbf{Y}|\mathbf{X})$ is small [12]. Here, we use KL divergence and suppose that $\mathbf{Y}$ can be partitioned into L disjoint groups $\mathbf{Y}_l$, i.e., $\mathrm{q}(\mathbf{Y}) = \prod_{l=1}^{L} \mathrm{q}(\mathbf{Y}_l)$; then, $\mathrm{q}(\mathbf{Y}_l)$ can be obtained in an alternating way by

$$\ln \mathrm{q}(\mathbf{Y}_l) = \mathbb{E}_{g \neq l}\left[\ln \mathrm{p}(\mathbf{Y}, \mathbf{X})\right] + \mathrm{const} \tag{9}$$

where $\mathbb{E}_{g \neq l}(\cdot)$ denotes the expectation with respect to q distributions over all variables $\mathbf{Y}_g$ for $g \neq l$.

Then, we apply variational Bayesian inference to the ship detection probabilistic model and have $\mathbf{Y} = \{\mathbf{A}, \mathbf{E}, \mathbf{S}, \mathbf{M}, \boldsymbol{\Lambda}, \boldsymbol{\omega}, \boldsymbol{\tau}, \mathbf{Z}, \boldsymbol{\pi}\}$, $\mathbf{X} = \mathbf{D}$. In this section, we will show the posterior distribution approximations of these latent variables. Since the priors of the latent variables are independent in the model, the approximations of the corresponding posterior distributions are also independent, i.e.,

$$\begin{aligned} \mathrm{q}(\mathbf{Y}) &= \mathrm{q}(\mathbf{A})\mathrm{q}(\mathbf{E})\mathrm{q}(\mathbf{S})\mathrm{q}(\mathbf{M}, \boldsymbol{\Lambda})\mathrm{q}(\boldsymbol{\omega}, \boldsymbol{\tau})\mathrm{q}(\mathbf{Z})\mathrm{q}(\boldsymbol{\pi}) \\ &= \prod_{i,j,k} \mathrm{q}(a_{ij})\mathrm{q}(e_{ij})\mathrm{q}(s_{ij})\mathrm{q}(\mu_{ij}, \lambda_{ij}) \\ &\qquad \cdot \mathrm{q}(\omega_k, \tau_k)\mathrm{q}(z_{ijk})\mathrm{q}(\pi_k). \end{aligned} \tag{10}$$

Thus, the factors in (10) can be calculated by substituting (8) into (9).

A. Estimation of $\mathbf{A}$ and $\mathbf{E}$

The posterior distribution approximation of each a_{ij} in $\mathbf{A}$ can be obtained by

$$\mathrm{q}(a_{ij}) = \mathcal{N}\left(a_{ij}|\mathbb{E}(a_{ij}), \sigma^2_{a_{ij}}\right) \tag{11}$$

with parameters

$$\begin{aligned}\sigma^2_{a_{ij}} &= \left(\sum_k \mathbb{E}(z_{ijk})\mathbb{E}(\tau_k)\mathbb{E}\left(s^2_{ij}\right)\right)^{-1}\\ \mathbb{E}(a_{ij}) &= \sigma^2_{a_{ij}}\left(\sum_k \mathbb{E}(z_{ijk})\mathbb{E}(\tau_k)\mathbb{E}(s_{ij})\left(d_{ij}-\mathbb{E}(\omega_k)\right)\right)\\ &\quad + \psi(\alpha_0)-\psi(\beta_0)\end{aligned} \tag{12}$$

where $\psi(\cdot)$ is the digamma function.

Similarly, the posterior distribution of each e_{ij} in $\mathbf{E}$ can be approximated by

$$\mathrm{q}(e_{ij}) = \mathrm{Beta}\left(e_{ij}|\alpha^*_0, \beta^*_0\right) \tag{13}$$

with parameters

$$\alpha^*_0 = \mathbb{E}(a_{ij}) + \alpha_0, \quad \beta^*_0 = \beta_0 - \mathbb{E}(a_{ij}) + 1. \tag{14}$$

B. Estimation of $\mathbf{S}$, $\mathbf{M}$, and $\mathbf{\Lambda}$

The posterior distribution of each s_{ij} in $\mathbf{S}$ can be approximated by

$$\mathrm{q}(s_{ij}) = \mathcal{N}\left(s_{ij}|\mathbb{E}(s_{ij}), \sigma^2_{s_{ij}}\right) \tag{15}$$

with parameters

$$\begin{aligned}\mathbb{E}(s_{ij}) &= \sigma^2_{s_{ij}}\sum_k \mathbb{E}(z_{ijk})\mathbb{E}(\tau_k)\mathbb{E}(a_{ij})\left(d_{ij}-\mathbb{E}(\omega_k)\right)\\ &\quad + \sigma^2_{s_{ij}}\mathbb{E}(\lambda_{ij})\mathbb{E}(\mu_{ij})\\ \sigma^2_{s_{ij}} &= \left(\sum_k \mathbb{E}(z_{ijk})\mathbb{E}(\tau_k)\mathbb{E}(a^2_{ij}) + \mathbb{E}(\lambda_{ij})\right)^{-1}.\end{aligned} \tag{16}$$

The posterior distribution of μ_{ij} and λ_{ij} can be approximated by

$$\begin{aligned}\mathrm{q}(\mu_{ij}, \lambda_{ij}) &= \mathcal{N}\left(\mu_{ij}|\mathbb{E}(\mu_{ij}), (1+\beta_1)^{-1}\mathbb{E}^{-1}(\lambda_{ij})\right)\\ &\quad \cdot \mathrm{Gam}\left(\lambda_{ij}|\alpha^*_1, \gamma^*_1\right)\end{aligned} \tag{17}$$

with parameters

$$\begin{aligned}\mathbb{E}(\mu_{ij}) &= \frac{1}{1+\beta_1}\left(\mathbb{E}(s_{ij}) + \beta_1\mu_{0ij}\right),\ \alpha^*_1 = \alpha_1 + 1\\ \gamma^*_1 &= \gamma_1 + \frac{\mathbb{E}\left(s^2_{ij}\right) - \beta_1\mu^2_{0ij}}{2} - \frac{\left(\mathbb{E}(s_{ij}) + \beta_1\mu_{0ij}\right)^2}{2(1+\beta_1)}.\end{aligned} \tag{18}$$

C. Estimation of $\mathbf{Z}$, $\boldsymbol{\pi}$, $\boldsymbol{\omega}$, and $\boldsymbol{\tau}$

The posterior distribution of each $\mathbf{z}_{ij}$ in $\mathbf{Z}$ can be approximated by

$$\mathrm{q}(\mathbf{z}_{ij}) = \prod_{k=1}^{K} \rho_{ijk}^{z_{ijk}} \tag{19}$$

with parameter $\rho_{ijk} = \xi_{ijk}/\sum_k \xi_{ijk}$, where

$$\begin{aligned}\ln \xi_{ijk} &= \frac{1}{2}\mathbb{E}(\ln\tau_k) - \frac{1}{2}\ln 2\pi + \mathbb{E}(\ln\pi_k)\\ &\quad - \frac{\mathbb{E}(\tau_k)}{2}\mathbb{E}(d_{ij} - a_{ij}s_{ij} - \omega_k)^2 + \mathrm{const}\\ \mathbb{E}(\ln\tau_k) &= \psi\left(\alpha^*_2\right) - \ln\left(\gamma^*_2\right)\\ \mathbb{E}(\ln\pi_k) &= \psi(\eta_{1k}) - \psi\left(\sum_k \eta_{1k}\right).\end{aligned} \tag{20}$$

The posterior distribution approximation of $\boldsymbol{\pi}$ is

$$\mathrm{q}(\boldsymbol{\pi}) = \prod_{k=1}^{K} \boldsymbol{\pi}_k^{\eta_{1k}-1} \tag{21}$$

with parameter

$$\eta_{1k} = \sum_{ij}\mathbb{E}(z_{ijk}) + \eta_{0k}. \tag{22}$$

The posterior distribution approximation of ω_k and τ_k is

$$\mathrm{q}(\omega_k, \tau_k) = \mathcal{N}\left(\omega_k|\mathbb{E}(\omega_k), \beta_k^{-1}\mathbb{E}^{-1}(\tau_k)\right)\cdot\mathrm{Gam}\left(\tau_k|\alpha^*_2, \gamma^*_2\right) \tag{23}$$

with parameters

$$\begin{aligned}\beta_k &= \sum_{i,j}\mathbb{E}(z_{ijk}) + \beta_2\\ \mathbb{E}(\omega_k) &= \frac{1}{\beta_k}\left(\sum_{ij}\mathbb{E}(z_{ijk})(d_{ij} - \mathbb{E}(a_{ij})\mathbb{E}(s_{ij})) + \beta_2\omega_{0k}\right)\\ \alpha^*_2 &= \alpha_2 + \frac{1}{2}\sum_{i,j}\mathbb{E}(z_{ijk}) + \frac{1}{2}\\ \gamma^*_2 &= \gamma_2 + \frac{1}{2}\left(\sum_{ij}\mathbb{E}(z_{ijk})\mathbb{E}(d_{ij} - a_{ij}s_{ij})^2 + \beta_2\omega^2_{0k}\right)\\ &\quad - \frac{1}{2\beta_k}\left(\sum_{ij}\mathbb{E}(z_{ijk})(d_{ij} - \mathbb{E}(a_{ij})\mathbb{E}(s_{ij})) + \beta_2\omega_{0k}\right)^2.\end{aligned} \tag{24}$$

D. Proposed Algorithm

The aim of ship detection is to estimate $\mathbf{A}$. Thus, this letter mainly focuses on $\mathrm{q}(\mathbf{A})$. However, (9) clearly shows that the estimation of $\mathrm{q}(\mathbf{A})$ depends on the expectations related to the other factors. Therefore, we first initialize all the factors appropriately and then update the estimation results of these factors in each iteration until convergence is reached. The complete procedure of the proposed ship detection algorithm is summarized in Algorithm 1. The initialization will be illustrated in Section IV-A.

The stopping criterion is

$$\frac{\left\|\mathbb{E}(\mathbf{A}^t \circ \mathbf{S}^t) - \mathbb{E}(\mathbf{A}^{t-1} \circ \mathbf{S}^{t-1})\right\|_F}{\left\|\mathbb{E}(\mathbf{A}^{t-1} \circ \mathbf{S}^{t-1})\right\|_F} < thres \tag{25}$$

where t denotes the tth iteration, $\|\cdot\|_F$ is the Frobenius norm, and $thres$ is the convergence threshold, which is set to be a small numerical constant [10]. The convergence of variational Bayesian inference is guaranteed in theory [12]. In our experiments, we find that $thres = 10^{-4}$ can guarantee the convergence of the proposed method after about ten iterations.

Algorithm 1 The Proposed Ship Detection Algorithm

Input: The input SAR image $\mathbf{D}$.
Initialization:
Initialize $\mathbf{Y}^0 = \{\mathbf{A}^0, \mathbf{E}^0, \mathbf{S}^0, \mathbf{M}^0, \mathbf{\Lambda}^0, \boldsymbol{\omega}^0, \boldsymbol{\tau}^0, \mathbf{Z}^0, \boldsymbol{\pi}^0\}$.
Initialize K, α_0, β_0, α_1, β_1, γ_1, α_2, β_2, γ_2, $\{\eta_{0k}\}$ and $thres$.
Iteration:
Set $t = 0$ and $thr = 2thres$.
while $thr > thres$ **do**
$t = t + 1$.
Estimate the posterior distributions of the latent variables with $\mathbf{Y}^{t-1}$ by (11)–(24).
Update $\mathbb{E}(\mathbf{Y}^t) = \mathbb{E}\{\mathbf{A}^t, \mathbf{E}^t, \mathbf{S}^t, \mathbf{M}^t, \mathbf{\Lambda}^t, \boldsymbol{\omega}^t, \boldsymbol{\tau}^t, \mathbf{Z}^t, \boldsymbol{\pi}^t\}$.
Update $thr = \|\mathbb{E}(\mathbf{A}^t \circ \mathbf{S}^t) - \mathbb{E}(\mathbf{A}^{t-1} \circ \mathbf{S}^{t-1})\|_F / \|\mathbb{E}(\mathbf{A}^{t-1} \circ \mathbf{S}^{t-1})\|_F$.
end while
Calculate $\widehat{\mathbf{A}}$ by (26).
Output: The final ship detection result $\widehat{\mathbf{A}}$.

When the iterative process converges, we let

$$\widehat{a_{ij}} = \begin{cases} 1 & e_{ij}^t \geq 0.5 \\ 0 & e_{ij}^t < 0.5 \end{cases} \tag{26}$$

because $\mathbb{E}(a_{ij}) = e_{ij}$. Then, the binary matrix $\widehat{\mathbf{A}} = [\widehat{a_{ij}}]$ is taken as the final ship detection result.

IV. Experiments

In this section, we first describe the selection of parameters in the proposed method. Then, we use synthetic data and a real RADARSAT-2 SAR image (see Fig. 1) to demonstrate the effectiveness of the proposed approach, which is compared with the traditional Gamma CFAR detector.

A. Parameter Setting

We take a simple method to initialize the variational Bayesian inference. We first calculate the empirical cumulative distribution of the input SAR image $\mathbf{D}$. Then, the pixel value corresponding to cumulative probability 0.6 is taken as the hard threshold. With this threshold, we can get the coarse detection result, and this result is used to initialize $\mathbf{A}^0$. $\mathbf{S}^0$ and $\mathbf{M}^0$ are initialized as $\mathbf{A}^0 \circ \mathbf{D}$. We set $\mathbf{E}^0$ to be all-ones matrix to indicate that $\mathbf{A}^0$ is not sparse with high probability. $\mathbf{\Lambda}^0$ is set to be all-ones matrix for indicating that $\mathbf{S}^0$ is not exact. As for the initialization of MOG, we find that five-component MOG is flexible enough to fit the sea clutter distribution, i.e., $K = 5$. Setting each ω_{0k} and ω_k^0 to be 0 is a common practice [12]. Each τ_k^0 is set to be 1 for the same reason like $\mathbf{\Lambda}^0$. Since we have no prior about the MOG, each $\mathbf{z}_{ij}^0$ is initialized as a random 1-of-K vector, and each π_k^0 is set to be $1/K$. To impose sparseness on $\mathbf{A}$, we set $\alpha_0 = 10^{-4}$ and $\beta_0 = 1 - \alpha_0$ [9]. The other hyperparameters α_1, β_1, γ_1, α_2, β_2, γ_2, and $\{\eta_{0k}\}$ are set to be 10^{-6} [8], [10].

B. Simulation Experiment

To demonstrate the robustness of the algorithm in detecting small and punctual targets, we first test the proposed method with synthetic data. We extract 100 ship points with average reflectivity σ_{ship}^0 ranging from -6.5 to -3.5 dB from Fig. 1.

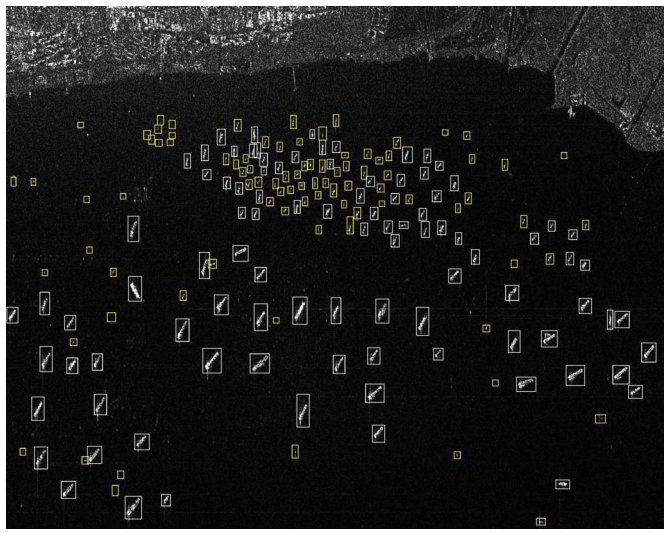

Fig. 1. C-band HH polarized SLC RADARSAT-2 SAR image acquired over the Singapore Strait area. Ground-truth ships, classified as big (B group) and small (S group) targets, are marked with white and yellow boxes, respectively.

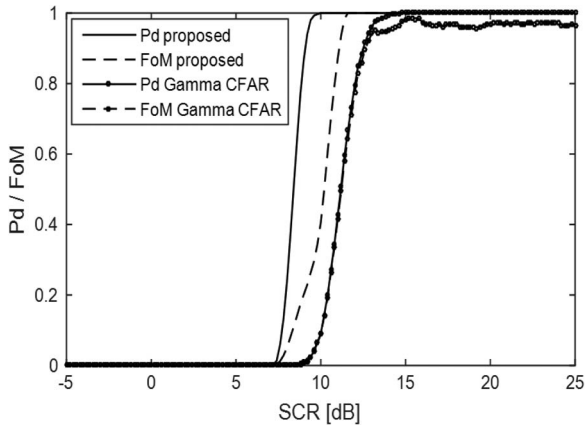

Fig. 2. Simulated results: Pd and FoM versus SCR.

Meanwhile, sea clutter is modeled by K distribution with the shape parameter $\nu = 1.33$ and the scale parameter $b = \nu/\sigma_{\text{sea}}^0$, where $\sigma_{\text{sea}}^0 = \overline{\sigma}_{\text{ship}}^0 - SCR$, $\overline{\sigma}_{\text{ship}}^0 = -4.7$ dB is the mean of σ_{ship}^0 and SCR denotes the signal-to-clutter ratio. Then, we let SCR increase from -5 to 25 dB and apply the proposed method and Gamma CFAR detector to the synthetic 200×200 single polarized SAR images. The parameters of the proposed method are set to be the values in Section IV-A. In the gamma CFAR detector, the size of the target, guard, and background areas in the sliding window are $w_t \times w_t$, $w_g \times w_g$, and $w_b \times w_b$, respectively ($w_t\_w_g\_w_b$ for short). Here, $w_t\_w_g\_w_b =$ 1_7_11, and Pfa $= 10^{-6}$. In order to quantitatively evaluate the detection performance, the detection probability P_d and the figure of merit FoM [13] are adopted

$$P_d = \frac{N_d}{N_g}, \quad FoM = \frac{N_d}{N_f + N_g} \tag{27}$$

where N_g is the number of ground-truth ships, N_f is the number of false alarms, and N_d is the number of detected ships. Fig. 2 shows the simulated result. It can be seen that the proposed method is superior than the Gamma CFAR detector.

TABLE I
SHIP DETECTION RESULTS

Method	$(N_d^{\mathrm{B}}, N_d^{\mathrm{S}})$	(N_d, N_f)	$P_d(\%)$	$FoM(\%)$
Proposed	(**94**, **69**)	(**163**, 5)	**88.6**	**86.2**
CFAR (7_79_91)	(82, 29)	(111,**1**)	60.3	60.0
CFAR (3_79_83)	(94, 55)	(149,15)	81.0	74.9

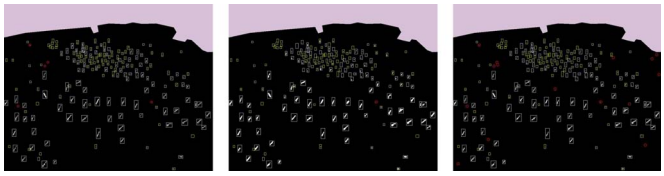

(a) (b) (c)

Fig. 3. Ship detection results with land masking. (a) Proposed approach. (b) CFAR (7_79_91). (c) CFAR (3_79_83). White boxes, yellow boxes, and red circles stand for B group ships, S group ships, and false alarms, respectively.

C. Experiment With RADARSAT-2 SAR Image

A C-band RADARSAT-2 polarimetric single-look complex (SLC) SAR image acquired over the Singapore Strait area is used. The image size is 1227 (slant range) $\times$ 2070 (azimuth) pixels. The nominal spatial resolution is 5.2 m (slant range) $\times$ 7.6 m (azimuth), and the pixel spacing is 4.7 m (slant range) $\times$ 4.8 m (azimuth). The incidence angle is about 47°. It should be noted that the original polarimetric SAR image is only used to get the ground truth. We use the HH polarized intensity image (see Fig. 1) to test the proposed method.

In the ground-truth definition, we use polarization information to assist in validating small ships and reducing the influence of azimuth ambiguity [11]. The final ground truth of ships marked with boxes is shown in Fig. 1, including 184 ships with a length of about 25–360 m. We classify these ships into two groups: The B group, which consists of 94 big ships with a length of about 125–360 m, is marked with white boxes in Fig. 1, and the S group, which consists of 90 small ships with a length of about 25–125 m, is marked with yellow boxes in Fig. 1.

The proposed method uses the same parameters as that in Section IV-A. In the Gamma CFAR detector, the Pfa is set to be 10^{-4}. According to the sliding-window setting regulation [1] and by observing the size of the ships in the input image, we set $w_t\_w_g\_w_b$ to be 7_79_91. In addition, we also provide another setup, 3_79_83, particularly setting $w_t = 3$ to improve the detection ability for small ships and setting $w_b = 83$ to avoid including surrounding ship pixels. A simple censoring approach is also adopted here, i.e., all the pixels in the background area are sorted in ascending order, and then, a quarter of pixels which correspond to high values are censored out.

Table I and Fig. 3 report the ship detection results by using the proposed method and the Gamma CFAR detector. In Table I, $N_d = N_d^B + N_d^S$, where N_d^B and N_d^S denote the number of detected ships in group B and group S, respectively. Referring to the results of P_d and FoM, we can find that the proposed method performs better than the Gamma CFAR detector whose performances improve in the setup configuration 3_79_83. Referring to the results of N_d^B and N_d^S, one can see that the proposed method is very effective in detecting small ships. In Fig. 3, we can also find that the proposed method can detect all of the 94 big ships in group B and 69 ships from the 90 small ships in group S. Moreover, it exhibits strong shape-preserving ability. Here, the shape refers to the distribution structure of the scatters on ships. By comparing the results in Fig. 3, we can see that the proposed method can capture the main scatters on ships, particularly for the ships in congested sea area, e.g., group S. Referring to the computational properties, the proposed method further shows high performances. In detail, processing the SAR image in Fig. 1 by MATLAB takes around 22.3 s, using a personal computer of Intel Core i7 processor with 3.40-GHz main frequency and 8.00-GB main memory. Thus, we can conclude that the proposed method can achieve state-of-the-art ship detection performance.

V. CONCLUSION

In this letter, a new ship detection method has been proposed. We have established the ship detection probabilistic model and introduced hierarchical priors in this model. Then, variational Bayesian inference has been employed to estimate the posterior distributions of the latent variables (including indicator variables of ships). The proposed approach is an iterative method without sliding windows and is beneficial to detect ships in congested sea areas. Simulation results show that the proposed method has higher P_d and FoM than the traditional Gamma CFAR detector. Experiments with the RADARSAT-2 SAR image further highlight that the proposed method has better shape-preserving ability. Future work will focus on the use of the spatial feature to preserve the shape of the detected ships.

REFERENCES

[1] D. J. Crisp, "The state-of-the-art in ship detection in synthetic aperture radar imagery" Intell., Surveillance, Reconnaissance Div., Inf. Sci. Lab., Edinburgh, SA, Australia, Tech. Rep. DSTO-RR-0272, May 2004.
[2] M. di Bisceglie and C. Galdi, "CFAR detection of extended objects in high-resolution SAR images," *IEEE Trans. Geosci. Remote Sens.*, vol. 43, no. 4, pp. 833–843, Apr. 2005.
[3] G. Gao, L. Liu, L. Zhao, G. Shi, and G. Kuang, "An adaptive and fast CFAR algorithm based on automatic censoring for target detection in high-resolution SAR images," *IEEE Trans. Geosci. Remote Sens.*, vol. 47, no. 6, pp. 1685–1697, Jun. 2009.
[4] W. T. An, C. H. Xie, and X. Z. Yuan, "An improved iterative censoring scheme for CFAR ship detection with SAR imagery," *IEEE Trans. Geosci. Remote Sens.*, vol. 52, no. 8, pp.4585–4595, Aug. 2014.
[5] Y. Cui, G. Zhou, J. Yang, and Y. Yamaguchi, "On the iterative censoring for target detection in SAR images," *IEEE Geosci. Remote Sens. Lett.*, vol. 8, no. 4, pp. 641–645, Jul. 2011.
[6] K. Ouchi, S. Tamaki, H. Yaguchi, and M. Iehara, "Ship detection based on coherence images derived from cross correlation of multilook SAR images," *IEEE Geosci. Remote Sens. Lett.*, vol. 1, no. 3, pp. 184–187, Jul. 2004.
[7] C. Brekke, S. N. Anfinsen, and Y. Larsen, "Subband extraction strategies in ship detection with the subaperture cross-correlation magnitude," *IEEE Geosci. Remote Sens. Lett.*, vol. 10, no. 4, pp. 786–790, Jul. 2013.
[8] Q. Zhao, D. Y. Meng, Z. B. Xu, W. M. Zuo, and L. Zhang, "Robust principal component analysis with complex noise," in *Proc. 31st ICML*, Beijing, China, 2014, pp. 55–63.
[9] X. H. Ding, L. H. He, and L. Carin, "Bayesian robust principal component analysis," *IEEE Trans. Image Process.*, vol. 20, no. 12, pp. 3419–3430, Dec. 2011.
[10] S. D. Babacan, M. Luessi, R. Molina, and A. K. Katsaggelos, "Sparse Bayesian methods for low-rank matrix estimation," *IEEE Trans. Signal Process.*, vol. 60, no. 8, pp. 3964–3977, Aug. 2012.
[11] C. Liu and C. H. Gierull, "A new application for PolSAR imagery in the field of moving target indication/ship detection," *IEEE Trans. Geosci. Remote Sens.*, vol. 45, no. 11, pp. 3426–3436, Nov. 2007.
[12] C. M. Bishop, "Approximate inference," in *Pattern Recognition and Machine Learning*, 1st ed. New York, NY, USA: Springer-Verlag, 2006.
[13] J. J. Wei, P. X. Li, J. Yang, J. X. Zhang, and F. K. Lang, "A new automatic ship detection method using L band polarimetric SAR imagery," *IEEE J. Sel. Topics Appl. Earth Observ. Remote Sens.*, vol. 7, no. 4, pp. 1383–1393, Apr. 2014.